International Journal of Thermophysics, Vol. 28, No. 3, June 2007 (© 2007)
DOI: 10.1007/s10765-007-0206-y

Benard–Marangoni Instability as Possible Modifier of Surface Alloy Composition

Y. W. Kim[1]

Thermophysical properties of amorphous alloys represent the features of a given material specimen, and, as such, they are dependent, in general, on their elemental composition. Some properties are measured at surfaces, and others are measured for the bulk as a whole. Complications arise when the elemental composition varies as a function of position within the material specimen, as demonstrated by simultaneous measurements of thermal diffusivity and elemental composition by time-resolved spectroscopy of laser-produced plasma (LPP) plume emissions. To further understand the source of a rather common near-surface elemental composition anomaly, the evolution of the surface composition of Wood's alloy under the influence of thermal cycling with, and without, a temperature gradient over the specimen has been investigated. Surface composition modifications have been found to take place by accumulation of irregularly spaced gray patches of an inhomogeneous composition on the surface in the presence of a temperature gradient. Determination of elemental composition by LPP spectroscopy shows the three-dimensional structure of the patches.

KEY WORDS: Benard–Marangoni instability; convection; near-surface composition anomaly; surface tension.

1. INTRODUCTION

The physics of thermophysical property determinations is complex because the measurement requires the combination of the thermodynamics of achieving a thermal state, compositional and morphological properties of a material specimen, and responsive sensing elements, as well as robust interplay among them all. This is plainly evident in the wide variability

[1] Department of Physics, Lewis Laboratory 16, Lehigh University, Bethlehem, Pennsylvania 18015, U.S.A. E-mail: ywk0@lehigh.edu

seen in the thermophysical property literature. Metallic alloys, including single-element specimens, exhibit high variability, for example, in spectral emissivity and thermal diffusivity. We have demonstrated that some of the variability can be traced to deviations of the near-surface elemental composition of one specimen to another of a given alloy [1]. This is a result of a new measurement method based on spectroscopy of laser-produced plasma (LPP) plume emissions. The total mass loss from the surface is directly related to the local thermal diffusivity, while the emissions at selected wavelengths provide the elemental composition and their time integral gives a measure of the total mass in the LPP plume [2, 3].

Of primary interest here is whether the reasons for development of a near-surface composition anomaly are intrinsic. We have documented for a model system of Wood's alloy that it is possible to drive the constituent elements across the alloy separately, and this would give rise to a complex temperature-dependent surface tension. We quench the two-dimensional (2-D) patterns of counter flowing surface cells, and perform repetitive applications of 2-D surface analyses by LPP spectroscopy. The resulting 3-D profiles of elemental composition are presented for a number of Wood's alloy specimens with several histories of thermal cycling.

2. EXPERIMENTAL SETUP

The experimental setup consists of a vacuum chamber that contains an open-top furnace at the lower end, optics for directing a high-power Q-switched laser pulse to the top surface of the Wood's alloy specimen within the furnace, and space to maintain a blanket of a neutral gas in order to impede the physical expansion of the laser-produced plasma (LPP) plume. Two electrical feedthroughs mounted on the base flange provide power to a Nichrome ribbon heater. Two gas feedthroughs provide the means to regulate the chamber pressure. In addition, the base flange, on which the specimen heating block is mounted, can be slided in two mutually orthogonal directions without breaking the vacuum seals by means of an x–y translation stage that is positioned outside the vacuum chamber.

The basic heating block consists of cylindrical copper stock. The top end of the solid copper cylinder has a machined recess in the form of a cylindrical indentation, 18.0 mm in diameter and 5.1 mm in depth. At the bottom end of the block, a diametrical through-hole has been drilled so that a Nichrome ribbon, 4.8 mm wide and 0.2 mm thick, can be routed through it and clamped with a machine screw. Heating of the block is accomplished by electrical heating of the ribbon with an ac electrical current up to 25 A. A blind hole has been drilled in the block and an

alumel–chromel thermocouple junction is inserted into the hole for measurement of the temperature of the block.

The crucible is a machined capsule and is placed inside the cylindrical recess of the heating block. A specimen is prepared by melting irregularly shaped rods of Wood's alloy in the crucible, which is made of either aluminum or boron nitride. Boron nitride turned out to be the best non-wetting material for the specimen, forming a meniscus along the edges at the lining. The crucible had outside dimensions of 17.8 mm in diameter and 5.1 mm in thickness. The crucible's interior volume was in the shape of a thin disk with a diameter of 16.3 mm or 17.5 mm, depending on whether an additional lining of boron nitride was used. The thickness of the molten specimen ranged from 0.4 mm to 3.8 mm as a control for imposing a thermal gradient on the specimen during a heating cycle.

An LPP plume is generated using a laser pulse of 25 ns full-width at half maximum intensity with a nominal power density of the order of $10^9\,\mathrm{W}\cdot\mathrm{cm}^{-2}$ on the focal area. The laser pulse is delivered through a focusing lens at the top of the vacuum chamber. The same lens and a high-power dichroic mirror gather the emissions from the LPP plume and direct them to a spectrograph. A second lens forms a one-to-one image of the plume onto a 10-μm wide entrance slit of the spectrograph. The exit plane of the spectrograph is equipped with a gated intensified array detector. The combined detection system facilitates measurement of the density of the surface matter by the constituent species; their elemental composition in mass% can be determined as a function of position along a line fixed by the entrance slit axis. There are 256 discrete positions that can be resolved over a distance of 6.35 mm along a line through the surface footprint of the plume. The footprint is an oblong area 2.3 mm long and 1.3 mm wide, and the laser power density is not uniform over the area, and therefore the individual photodetector elements of the array detector must be calibrated.

The specimen can be moved over a 3 mm by 3 mm area by means of an x–y translation stage to better than one micron resolution. Surface elemental composition analysis is achieved, however, by resolving emission spectra within the footprint of the LPP plume, not by a point-by-point mapping. This is because there is a non-trivial chance that nano-particles resulting from one LPP plume can settle on the area adjacent to the focal spot [4]. The translation capability is thus used only to explore different surface areas of interest on a given specimen. More details of the experimental setup may be found in an accompanying article [5].

The ambient gas medium plays two important roles: (a) confinement of the LPP plume by collisions of the gas atoms with the metallic elements entrained into the plume and (b) definition of the temperature at the top

surface of the melt by transporting the heat away from the top surface, in contrast to the bottom surface that facilitates heating. Throughout this study, we have started the experiment by evacuating the vacuum chamber and filling it with argon to one atm. For a long sequence, the chamber is evacuated and refilled with argon in order to purge the build-up of metallic nano-clusters that result from cooling of the LPP plumes [4].

3. PROTOCOL FOR HEATING CYCLES

The central question of interest in this study involves identification of the primary mechanism responsible for the development of the near-surface elemental composition anomaly during thermal cycling of the specimen. We have seen that there is a threshold temperature above which the anomaly becomes permanent. Whether this pertains to a condition for stable alloy formation of Wood's metal or to the existence of a threshold for the onset of convection in the melt was unknown at the start of the study. Of course, the manner by which the anomaly emerges was of great interest; it was also unknown whether the anomaly develops uniformly across the free surface or in a position-dependent manner.

The experimental strategy was coarsely grained first to heat the specimen with, and without, a thermal gradient so that the study would demonstrate or provide evidence for the roles of alloy stability versus fluid instability in the melt. We chose the temperature range to be between room temperature and 393°C. We also decided that a specimen was to be cycled through a fixed heating schedule over the temperature range more than once, instead of a single slow cycling.

The aspect ratio of the specimen has been increased to widen the dynamic range of the thermal control parameter. In the original experiment, the specimen was 9.0 mm in diameter and 6.4–9.5 mm in thickness [2], whereas in the present study the specimen diameter is doubled and the thickness reduced more than 10-fold. An insulating lining of boron nitride may be added to the side of the crucible to reduce thermal conduction by the crucible walls and to maximize thermal gradients when appropriate.

4. EXPERIMENTAL RESULTS AND ANALYSIS

For greater depth control of the melt, the specimens were prepared from disks cut from Wood's alloy slabs that were made by rolling thin lumps in a rolling mill to different thickness: 0.4, 0.8, and 2.5 mm. Disks were punched out and stacked to the desired thickness.

Initial attempts included use of tracer particles for visualization of convection patterns in the melt. Fine mesh black powders of iron oxide

were sandwiched between specimen disks near the bottom of the specimen in the crucible. This approach was abandoned because molten Wood's metal failed to wet the iron oxide particles and the particles changed color to rust red due to heating.

The two most definitive thermal cycling schemes were (*a*) to heat the specimen at a modest rate in the crucible with the crucible open at the top to the atmosphere of argon at one atm and (*b*) to heat at the same rate with the crucible top closed by encasing the crucible and the heater block in an aluminum cover. A moderate rate of heating as used here means to raise the temperature of the specimen from room temperature to 393°C in 13–15 min, and when the peak temperature is reached, the heater power is turned off. The intent is to maximize the temperature gradient in scheme *a* or to minimize or eliminate the temperature gradient throughout the specimen in scheme *b*. The primary findings from scheme *a* are as follows: (i) the top surface of the specimen began to show discrete gray patches of discoloration at the end of the first heating; (ii) the number and size of the patches, as well as the shades of darkness increased with the number of heating cycles; this tendency was affected inversely by the initial thickness of the specimen; (iii) the positions of the patches did not show symmetric regular patterns, as typically seen in Rayleigh–Benard experiments carried out with transparent normal liquids [6–8]; (iv) the free surface of the specimen remains rough midway into heating; (v) the top surface of the melt responded to mechanical stimuli as though the surface was covered with a thin solid membrane; and (vi) heating of a specimen in an aluminum crucible showed disjointed dark spots, which become connected at subsequent cycles of heating. The result from scheme *b* is clear: no gray patches appeared at the end of heating, and the specimen appeared as bright as any fresh specimen.

Figure 1 shows scanned images of the specimens with and without discolored patches. The near-surface composition anomaly seems to be a result of the modifications forced on the specimen's elemental composition by aggregates of the patches. We have thus focused on gauging the physical scale of the patches, i.e., the sizes in three mutually orthogonal directions by means of time-resolved spectroscopy of LPP plumes. This is done by generating LPP plumes repetitively from a fixed surface point and tracking the changes in the spectroscopic signatures as a function of the LPP shot number.

Surface position-resolved detection of elemental composition is accomplished first by focusing the one-to-one image of the footprint of the LPP plume on the plane of the entrance slit of the spectrograph. The 10-μm wide slit is imaged onto the exit plane of the spectrograph on the 2-D gated intensified array detector. The result is that up to 256 emission

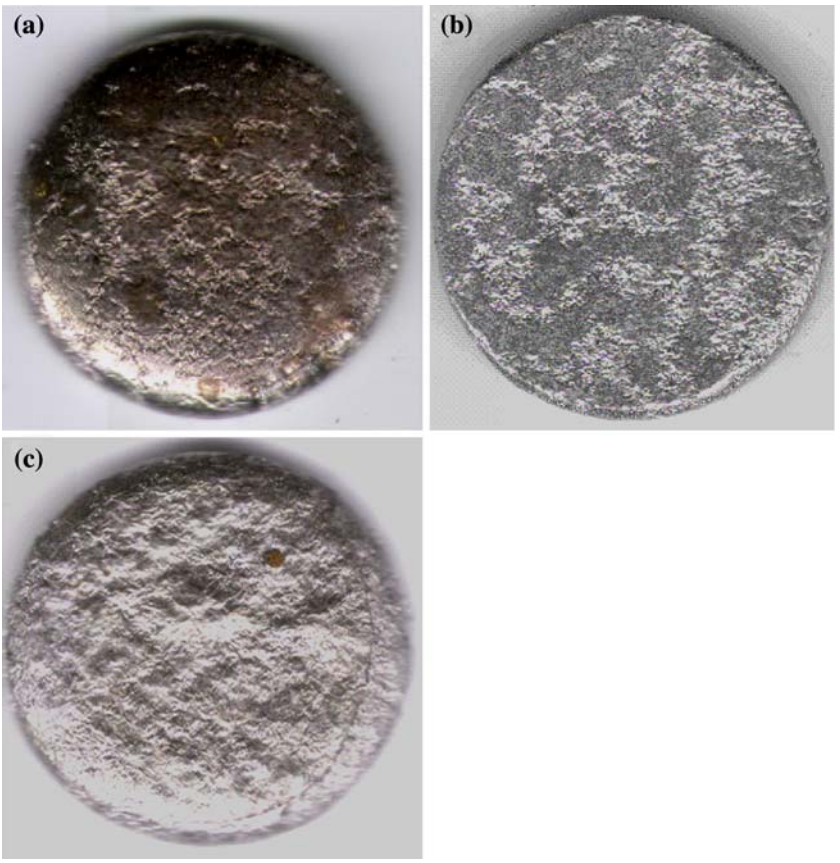

Fig. 1. (a) Scanned image of the top surface of a 2.5 mm thick Wood's alloy specimen that was treated through one round of the 13-min heating cycle to 393°C when the crucible was held in the heating block with its top surface exposed to the blanket of argon at one atm; and (b) and (c) scanned images of the bottom and top surfaces, respectively, of another Wood's alloy specimen when the crucible and the heater block were encased within a blind cylindrical cover of aluminum during the same heating cycle as in (a).

spectra are captured, one each from each individual surface point along the surface line segment at a selected time window. The intensities are calibrated against those of a pure specimen as a standard; the elemental composition is thus obtained as a function of position along the line. When repeated, we obtain the elemental composition measurement at increasing depth from the surface because each laser pulse removes a definite thickness of specimen matter. More detailed discussions of the calibration and

the procedure for determination of elemental composition may be found elsewhere [1–3, 5].

The surface patches can be individually selected for analysis by translating them into the focal area of the laser pulse and imaging them in the manner described above. Figure 2a shows the percent change in mass% at 100 different surface points along a line cutting across a patch relative to the reference specimen; Fig. 2b shows the elemental composition of the top surface layer as a function of position. The resulting elemental composition profile is shown in Fig. 3 for one of the patches for 100 points along a line through the patch at ten different depths from the surface. On average, the mass loss from the surface is 2.71 μg/pulse and the thickness of surface matter removed is 0.12 μm per laser pulse. A significant depth may be explored in this way.

The results show that the thickness of this particular patch is about four LPP ablations deep. In the topmost layer and the next layer below, one can see the evidence of enrichment in cadmium, whereas the increase in bismuth extends over several layers. Cadmium enrichment becomes further accentuated with an increase in the number of thermal cycles.

5. DISCUSSION AND CONCLUSIONS

The experimental observations indicate that a temperature gradient is a critical requirement for the development of a near-surface composition anomaly during thermal cycling of Wood's alloy specimens. This would suggest convection within the melt, which is normally described within the framework of Benard–Marangoni instability. The Benard–Marangoni instability has two driving mechanisms: buoyancy arising from the temperature dependence of the mass density of a molten metal and the temperature dependence of the surface tension [9, 10]. Experiments carried out in transparent liquids on the Rayleigh–Benard instability, where buoyancy dominates, show emergence of roll or cellular patterns of convection near the threshold of convection instability [6–8]. When the surface tension effect is strong, the Marangoni instability emerges, revealing depressions in the free surface that are geometrically irregular, supposedly, due to domination of the long wavelength surface convection mode near the instability threshold [11]. This might be viewed as descriptive of the Wood's alloy experiment here.

The question as to why strong enrichment of cadmium takes place in the surface layers remains unanswered. The fact that Wood's alloy is a low melting-point metal, well below the melting points of the constituent alloying elements of bismuth, lead, tin, and cadmium, suggests that the elemental species are strongly coupled in the normal state of the alloy.

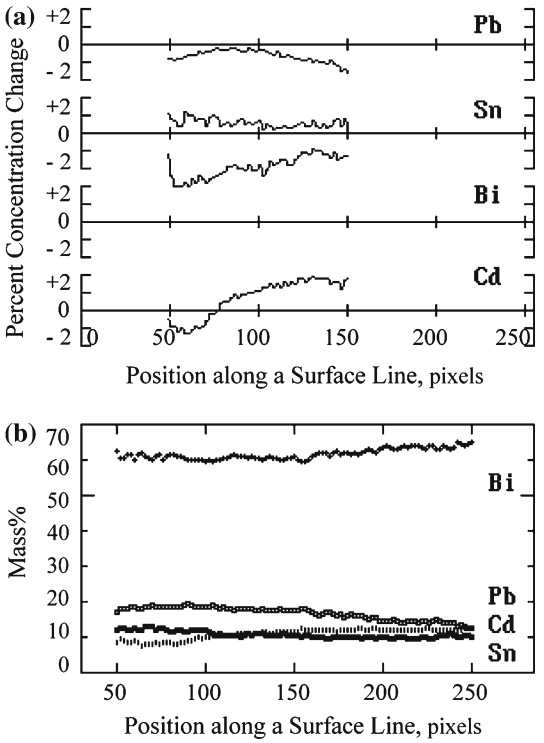

Fig. 2. (a) Percent changes in elemental concentration in the topmost layer of a Wood's alloy specimen along a 2.48-mm long line that cuts across a discolored surface patch, as compared with a fresh specimen. Two identical laser pulses are used to excite the topmost surface layer of the specimen and the reference specimen. Quantitative analysis of the two sets of emissions from the two LPP plumes produced the percent changes in the elemental concentration. (b) Calibrated mass% of the topmost layer of the thermally cycled specimen is shown for four different constituent elements, bismuth (crosses), lead (squares), cadmium (lines), and tin (filled squares), as functions of detector pixel address. Two adjacent detector pixels are separated by 24.8 μm along the line.

These elements may have to segregate at the surface in order for large enrichment of cadmium to occur. This, in turn, will drive not only quantitative changes of surface tension but also a functional relationship of surface tension and the melt temperature. Disparate pieces of observations on hand and the above analysis suggest that the convection instability

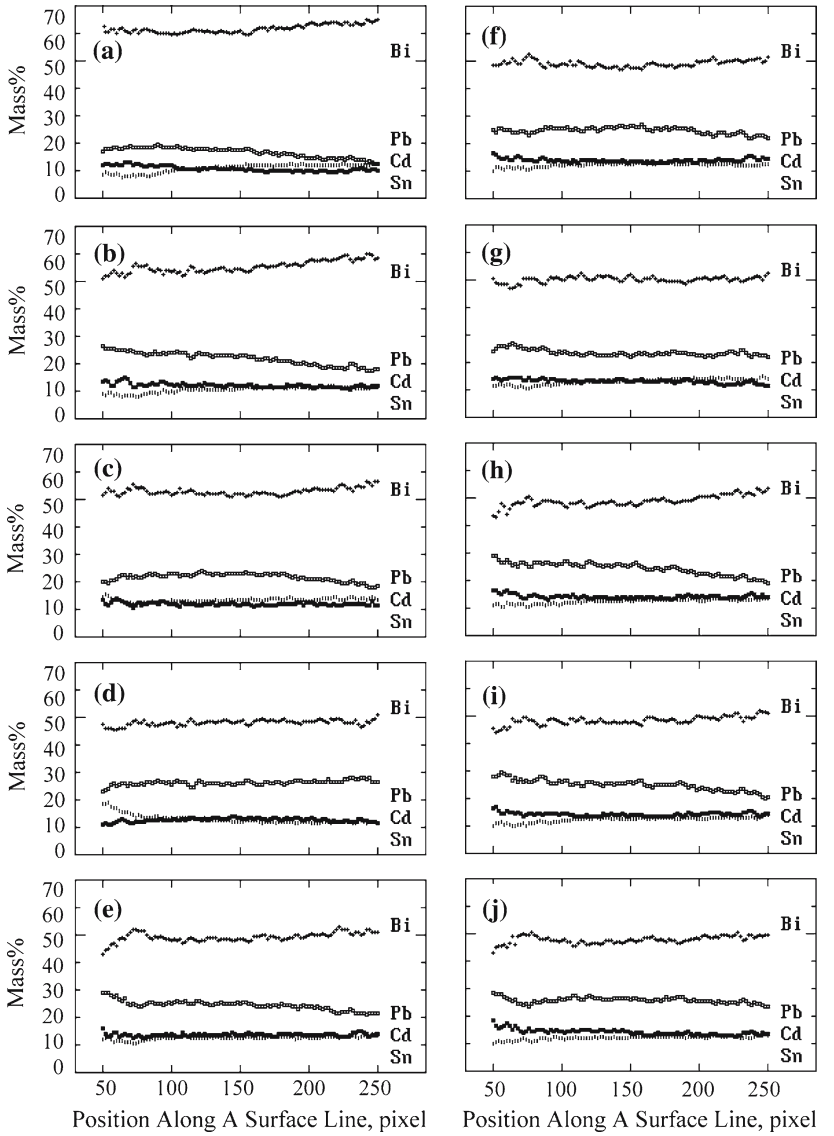

Fig. 3. Position-resolved elemental mass% values are shown for ten successive layers, going from the topmost surface layer (a) to the tenth layer (j), at one of the surface patches of the same thermally cycled Wood's alloy specimen of Fig. 2. Four constituent elements are tracked as a function of adjacent points along a line cutting through the cross section of the patch: bismuth (*crosses*), lead (*squares*), cadmium (*lines*), and tin (*filled squares*). Succeeding specimen layers, each ablated by a laser pulse, are separated on average by 0.12 μm in depth.

is primarily driven by the surface tension. Thermophysical property data of Wood's alloy are scarce and sketchy at present in that their temperature dependences are unknown. This state of affair applies to: thermal conductivity at the melting point [12], solid versus liquid mass density, heat capacity, and latent heat of melting [13]; and surface tension, kinematic viscosity, and mass density [14]. The absence of more detailed property data makes it difficult to test the applicability of instability theory. A model for calculation of the surface tension for molten multi-element alloys near their solidification points is needed.

It is also possible that the particular Wood's alloy specimens contained small granules of pure cadmium. These grains floated to the surface of the melt, assisted by the convective instability, and when the melt temperature reached the critical temperature, the grains melted and diffused to form the patches. Any unambiguous resolution of such a possibility will benefit from a reasonable phase diagram for the four-element Wood's alloy.

These issues at hand are certainly interesting and, perhaps, crucial to the development of a comprehensive understanding of how the elemental composition profile of alloy specimens evolves. Whatever the elemental transport processes may be in the molten state of a specimen, alloy specimens at room temperature are affected by the same physics although at much lower transport rates. In addition, each specimen at a nominal alloy composition may have been imprinted with a different elemental composition profile depending on a particular processing history. In the end, the robustness of thermophysical property data hangs in the balance. Much more theoretical and experimental investigation seems in order.

REFERENCES

1. Y. W. Kim, *Int. J. Thermophys.* **26**:1051 (2005).
2. Y. W. Kim, *Int. J. Thermophys.* **25**:575 (2004).
3. Y. W. Kim, in *Thermal Conductivity* **26**, R. B. Dinwiddie, ed. (DES*tec* Pubs, Lancaster, Pennsylvania, 2005), pp. 146–158.
4. Y. W. Kim, H.-D. Lee, and P. Belony, Jr., *Rev. Sci. Instrum.* **17**:10F115 (2006).
5. Y. W. Kim, *Int. J. Thermophys.* doi: 10.1007/s10765-007-0171-5.
6. T. Ondarçuhu, G. B. Mindlin, H. L. Mancini, and C. Peréz-García, *Phys. Rev. Lett.* **70**:3892 (1993).
7. T. Ondarçuhu, G. B. Mindlin, H. L. Mancini, and C. Peréz-García, *J. Phys.: Condens. Matter* **6**:A427 (1994).
8. S. Hoyas, A. M. Mancho, H. Herero, N. Garnier, and A. Chiffaudel, *Phys. Fluids* **17**:054104-1 (2005).
9. M. I. Char and C. C. Chen, *J. Phys. D: Appl. Phys.* **30**:3286 (1997).
10. M. I. Char and K. T. Chiang, *J. Phys. D: Appl. Phys.* **27**:748 (1994).
11. S. J. VanHook, M. F. Schatz, J. B. Swift, W. D. McCormick, and H. L. Swinney, *J. Fluid Mech.* **345**:45 (1997).

12. W. M. Rohsenow, J. P. Hartnett, and Y. I. Cho, eds., *Handbook of Heat Transfer* (McGraw Hill, New York, 1998), p. 2.63.
13. M. Lamvik and J. M. Zhou, *Meas. Sci. Technol.* **6**:880 (1995).
14. M. Iguchi and H. Tokunaga, *Metall. Mater. Trans. B* **33B**:695 (2002).